Joint Light Planning and Error-Rate Prediction for Dual-Use Lighting/Visible Light Communication

Jan Mietzner, *Senior Member, IEEE*, Andrej Harlakin, Peter A. Hoeher, *Fellow, IEEE*, Tina Fast, Carolin Liedtke, Robert Heinze, and Roland Greule

***Abstract*—We consider error-rate prediction for dual-use lighting systems with visible light communication (VLC) functionality. Since *light planning* rather than communications engineering is usually the driving discipline for practical dual-use settings, we extract VLC channel parameters as a by-product from advanced 3-dimensional (3D) light-planning models. By this means, we attain realistic signal-to-noise ratios for exemplary positions of a VLC receiver, which allows us to predict corresponding end-to-end bit error rates (BERs). Specifically, our procedure accounts for important aspects of state-of-art lighting systems, such as realistic light distribution curves of employed luminaires, possible presence unmodulated light sources, and, particularly, adaptive dimming operations in response to prevalent sunlight. In this paper, we (i) devise a methodology for VLC systems with optical receive filtering to convert photometric quantities into radiometric quantities, (ii) present examples of BER predictions for selected modulation schemes within some basic office environments, and (iii) conduct an analysis of the resulting simulation accuracy for a particular 3D light-planning tool. Simulation results show that our approach is indeed suited to predict realistic end-to-end BERs for dual-use lighting/VLC systems. Moreover, our procedure is fairly general and may be tailored to specific practical office settings and particular light plans of interest.**

***Index Terms*—Wireless communication, visible light communication, lighting, lighting control, optical communication equipment, channel models.**

I. Introduction

VISIBLE light communication (VLC) as an alternative to radio-frequency (RF) solutions has attracted considerable interest in recent years both in academia and industry [1], [2], [3], [4]. VLC is an instant of optical wireless communication (OWC) [5], [6], [7] and utilizes the visible part of the electromagnetic spectrum. If fully connected and bidirectional, VLC/OWC is referred to as Light Fidelity (LiFi). Corresponding standardization efforts have been underway for several years now [8], [9] and have paved the way to first commercially available products. Among several advantages over RF systems, VLC systems offer the potential of very high data rates for short- to medium-range wireless links, unlicensed spectrum usage, better electromagnetic compatibility, and an increased physical-layer security [4, Ch. 1.2]. In the context of quantum networking, it is anticipated that even additional security on the physical layer of VLC systems can be achieved, for example by means of quantum key distribution [10]. A particular advantage of VLC systems is that in downlink direction existing lighting systems may be reused for wireless communication, thus offering a cost-effective backbone infrastructure. This is particularly interesting for office environments, where considerable effort is usually spent on light planning, in order to meet ergonomic lighting requirements for each workspace. At the same time, this offers the potential of dedicated broadband optical wireless connectivity exactly at those locations, where it is most required.

Various publications have addressed aspects of channel modeling for (indoor) VLC, in order to describe the properties of the physical channel from the perspective of communications engineering [11], [12], [13], [14], [15], [16], [17], [18], [19], [20]. Such channel models focus – per definition – on the *communications function* of joint lighting/VLC systems and offer valuable insight into the physical mechanisms of VLC signal propagation. For example, it is found that (higher-order) reflection paths may contribute significantly [15]. Correspondingly, multipath signal propagation needs to be taken into account, in order to predict realistic signal-to-noise ratios (SNRs) at the receiver, to capture possible intersymbol interference (ISI) effects, and to study non-line-of-sight (NLoS) communication scenarios. Yet, often aspects regarding the *lighting function* of joint lighting/VLC systems are not fully captured by these models. For example, light-emitting diodes (LEDs) are often modeled as (ideal) generalized Lambertian sources, which usually does not sufficiently represent angular light distribution curves (LDCs) of practical LEDs. This also poses limitations from a communications engineering perspective, since the available signal energies at the receiver – and thus resulting bit error rates (BERs) – might not be predicted accurately [19]. Another aspect relevant for practical joint lighting/VLC systems concerns interference effects caused by additional (unmodulated) light sources – for example sunlight illuminating parts of the

Manuscript received 7 October 2022; revised 21 November 2022; accepted 26 November 2022. Date of publication 30 November 2022; date of current version 8 December 2022. *(Corresponding author: Jan Mietzner.)*

Jan Mietzner, Tina Fast, Carolin Liedtke, and Roland Greule are with the Hamburg University of Applied Sciences, Faculty of Design, Media, and Information, D-22081 Hamburg, Germany (e-mail: jan.mietzner@haw-hamburg.de; tina.fast@haw-hamburg.de; carolin.liedtke@haw-hamburg.de; roland.greule@haw-hamburg.de).

Andrej Harlakin and Peter A. Hoeher are with the Kiel University, Faculty of Engineering, Chair of Information and Coding Theory, D-24143 Kiel, Germany (e-mail: anha@tf.uni-kiel.de; ph@tf.uni-kiel.de).

Robert Heinze is with the Relux Informatik AG, CH-4142 Muenchenstein, Switzerland (e-mail: r.heinze@relux.com).

Digital Object Identifier 10.1109/JPHOT.2022.3225708

working environment or artificial light sources put into place, in order to complete the overall lighting design. Furthermore, state-of-art lighting systems are *adaptive* systems [21] able to adjust to prevailing sunlight conditions – with the goal to provide a constant illumination level for workspaces by dimming LEDs to a level just sufficient to meet ergonomic lighting requirements and to avoid dazzle effects. Such dimming operations have a direct effect on the available signal energy at the VLC receiver and should therefore be incorporated in the overall VLC model. On the other hand, aspects of practical VLC systems – concerning, for example, optical filtering techniques and electrical bandwidths of practical LEDs – should also be incorporated, in order to arrive at a realistic end-to-end model.

In fact, for joint lighting/VLC systems the lighting function is usually the primary one [2], [3], [4], whereas the communications function is subordinated as an additional dual-use feature. Correspondingly, *light planning* rather than communication channel modeling is the driving design discipline in such settings. To this end, light planners employ corresponding tools for 3-dimensional (3D) visualization of resulting light atmospheres – without considering any VLC channel modeling aspects in the first place. Yet, professional light-planning tools, such as ReluxDesktop [22], Zemax OpticStudio [23], or DIALux [24] are able to model complex indoor settings and predict resulting light intensities found across any given test surface within the 3D simulation model. The primary purpose is to simplify light planning procedures, e.g., for designing workspaces with regard to ergonomic lighting requirements, as time-consuming and costly in-place measurements may be complemented or entirely replaced by simulations. However, regarding the VLC part, the *same* 3D simulation setup may also serve as a starting point for end-to-end error rate prediction, when a test surface of suitable size is thought to represent the area of a corresponding VLC photo detector. By this means, error rate prediction can be tailored to particular office settings, specific light plans of interest, and exemplary positions of an VLC receiver.

The idea to use a light planning/optical design tool as a starting point for VLC channel modeling was pursued in [25], [26], which is – to the best of our knowledge – the only example found in the literature. The focus of these papers was on identifying key parameters for VLC channels and incorporating them into the IEEE 802.15.7r1 reference channel models. In particular, notable differences to infrared (IR) channel models were pointed out, which derive from the fact that the visible part of the electromagnetic spectrum is associated with a considerably larger optical bandwidth than the IR spectrum, thus leading to wavelength-dependent reflection characteristics. Correspondingly, the general assumption for these VLC channel models was that the entire optical bandwidth (or at least a large fraction of it) is utilized for VLC signaling. Aspects of limited optical bandwidths in practical VLC systems were not taken into account in [25], [26], and end-to-end performance predictions were also not considered.

For illumination purposes – especially in office environments – white LEDs are currently most relevant. Technically, white LEDs are realized either by mixing the light generated by multiple monochromatic LEDs or by employing a single blue core LED coated with a phosphor layer.[1] The phosphor coating generates a wide-band optical spectrum via stimulated emission, which yields a (warm, neutral, or cold) white color impression. Among these two options, phosphorescent white-light LEDs are characterized by a more favorable color rendering index (CRI) [4, Ch. 2.4] and are therefore usually preferred for office and other environments requiring high-quality lighting systems. Regarding VLC, however, the phosphor coating is rather undesired, because it entails slow response times, which severely limits achievable data rates. Therefore, corresponding VLC receivers usually employ an optical filter tailored to the blue core LED [27]. By this means, the influence of the phosphor can be largely eliminated from the modulated light signal, so that higher data rates can be attained by employing faster switching times. Correspondingly, with phosphorescent white-light LEDs effectively only the blue part of the optical spectrum is exploited for VLC data transmission, while the electrical bandwidth of the blue core LED is typically limited to a value of about 20 MHz [4, Ch. 3.2].

In this paper, we consider end-to-end BER prediction for high-quality dual-use lighting/VLC systems based on 3D light planning simulations. Our main contributions are as follows:

- We develop a realistic end-to-end VLC model by incorporating key parameters of a VLC system, including a limited optical and electrical bandwidth.
- For the case of phosphorescent white-light LEDs, we devise a methodology to convert photometric quantities into radiometric quantities and derive an analytical expression for the end-to-end SNR at the VLC receiver, incorporating adaptive dimming operations as well as possible interference caused by unmodulated light sources.
- We present examples of BER predictions for selected modulation schemes within some basic office environments, which are based on the 3D light planning simulation tool ReluxDesktop [22] – including realistic LDCs as well as higher-order signal reflections.
- We conduct an analysis of the resulting simulation accuracy attained with ReluxDesktop, which shows that our approach is indeed suited to predict realistic end-to-end BERs for high-quality dual-use lighting/VLC systems.

The remainder of the paper is organized as follows: In Section II, some preliminaries are discussed and the underlying VLC transmission model is introduced. Analytical expressions for the end-to-end SNR at the VLC receiver are derived in Section III. End-to-end BER prediction examples for some basic office settings using ReluxDesktop are presented in Section IV, where focus is on on-off keying (OOK) and pulse-position modulation (PPM). Furthermore, the attained accuracy of the simulation results is illustrated for selected examples. Finally, conclusions are drawn in Section V, and possible directions for future work are highlighted.

[1]We note that practical LEDs are not truly monochromatic, but comprise a certain optical bandwidth. Correspondingly, the term "quasi-monochromatic" might be more appropriate.

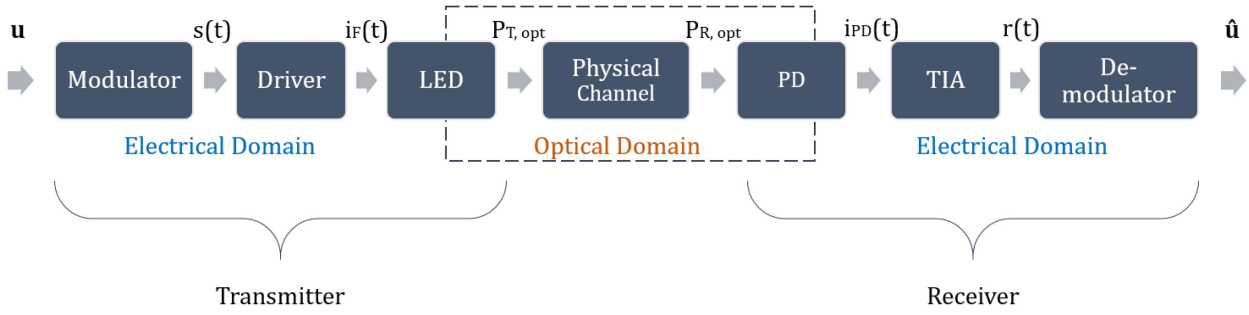

Fig. 1. VLC transmission scheme including modulation and demodulation.

II. Preliminaries

Throughout this paper, we consider a phosphorescent white-light LED-based dual-use lighting system with VLC functionality. As pointed out in the Introduction, such LEDs are well suited for (moderate-rate) VLC applications and are widely used in modern high-quality lighting systems – due to their high energy efficiency and favorable CRI.

A. VLC Transmission Model

Regarding VLC, we focus on simple single-carrier modulation schemes as an example – namely OOK and (Variable) PPM. Fig. 1 illustrates the underlying system model for the VLC part according to [4, Ch. 3.6]. In the electrical domain, the transmitted bit sequence $\mathbf{u}$ is first modulated onto an analog transmit signal $s(t)$, which is passed to a transmit driver. The output current $i_{\mathrm{F}}(t)$ of the transmit driver feeds the LED, which emits a corresponding light signal with average optical power $P_{\mathrm{T,opt}}$. In the optical domain, the emitted light signal propagates through the physical channel and is captured by a photo detector (PD) at the receiver – typically a positive-intrinsic-negative (PIN) photo diode. The PD converts the received light signal with average optical power $P_{\mathrm{R,opt}}$ back to the electrical domain and yields a corresponding output current $i_{\mathrm{PD}}(t)$. A transimpedance amplifier (TIA) finally yields the received signal $r(t)$, which is demodulated to obtain the estimated bit sequence $\hat{\mathbf{u}}$ (channel coding is not considered for simplicity, but may be incorporated). Note that the dynamic range of the TIA must be sufficiently large (and the operating point of the PD output current adjusted accordingly), in order to avoid undesired saturation effects. For the blue core LED, an electrical bandwidth of $B_{\mathrm{LED,el}} \leq 20$ MHz is assumed in the sequel. Moreover, an optical bandpass filter is assumed at the receiver, which is tailored to the optical spectrum of the blue core LED (e.g., the wavelength region 430 nm – 470 nm).

An important aspect is how to handle ambient light in a practical VLC system. One option is to employ a liquid-crystal display (LCD) as an optical receive filter unit [28], [29]. In this paper, we assume that the driver circuit includes a mixing step to some carrier frequency $f_c > 0$ Hz, so that the data signal in the electrical domain can be separated from ambient (unmodulated) light found at direct current (DC), i.e., at frequency $f = 0$ Hz. This is accomplished by means of a corresponding bandpass filter (BPF) with single-sided bandwidth $B_{\mathrm{filt,el}} \geq B_{\mathrm{LED,el}}$ placed after the PD (not depicted). Furthermore, the demodulator is assumed to include another (digital) filtering step, namely a matched filter with single-sided bandwidth $B_{\mathrm{MF}} \leq B_{\mathrm{filt,el}}$ tailored to the employed pulse shape of the underlying modulation scheme.

B. 3D Light-Planning Tool

Within the scope of this paper, we focus on ReluxDesktop (Version 2020.2.5.0) [22], which is a professional 3D lighting simulation and visualization tool employed for indoor and outdoor light planning tasks. In particular, it features many functions tailored to typical workflows used by light-planning architects, includes a large data base of available luminaire and their corresponding LDCs, and is able to simulate both artificial and natural light – incorporating even geographic information for maximal realism. Office or general room settings can be created directly within ReluxDesktop or can be imported as computer-aided design (CAD) data. To create complex settings, walls, doors, windows, and furniture can be placed freely within basic settings, and various material and reflection properties of corresponding surfaces may be chosen. Moreover, test surfaces may be placed within the setting at arbitrary positions and with arbitrary orientation. This enables corresponding "measurements" of light intensities within the 3D simulation at selected locations of interest.

ReluxDesktop comprises two different computation kernels – a ray-tracing kernel, which includes different reflection types (diffuse, specular, and mixed reflections), and a radiosity kernel adopted from the field of computer graphics [30], which is tailored to diffuse reflections. Both kernels may be used for simulating light propagation within a chosen 3D setting and assessing corresponding light-intensities, while the radiocity kernel also serves for visualizing resulting light atmospheres with realistic optical impressions. Within the scope of this paper, we will focus on the radiosity kernel, as we are mainly interested in an end-to-end analysis of received SNRs and corresponding BERs. For a detailed analysis of VLC channel model parameters – e.g. along the lines of [25], [26] – the ray-tracing kernel could yield additional insights, however. In future work, the radiocity kernel might also be extended to account for signal propagation delays, e.g., following the frequency-domain approaches described in [15], [18].

Basically, the current radiosity kernel incorporates a physical optics model and deals with the exchange of luminous fluxes between surfaces within the 3D model. In particular, the luminous flux fraction $\Phi_{i,j}$ in Lumen (lm) across a surface A_j, which is contributed by another reflecting surface A_i, can be calculated via numerical integration according to

$$\Phi_{i,j} = \int_{A_i} \int_{A_j} L_i \, \frac{\cos(\phi_i)\, \mathrm{d}A_i \cdot \cos(\phi_j)\, \mathrm{d}A_j}{r_{i,j}^2}, \qquad (1)$$

where L_i denotes the luminance in lm/(sr m^2) associated with area increment $\mathrm{d}A_i$ (sr: steradian), ϕ_i and ϕ_j denote the angles between the connecting line of area increment $\mathrm{d}A_i$ and $\mathrm{d}A_j$ and the respective area normal vectors, and $r_{i,j}$ denotes the distance between $\mathrm{d}A_i$ and $\mathrm{d}A_j$ in m. Correspondingly, for a given (plane) test surface within the 3D simulation setup, ReluxDesktop provides resulting illuminance values E_V in lux (lx) (= lm/m^2). Note that the radiosity kernel currently employs solely *photometric* quantities. While in the future this may be extended to radiometric quantities, our analytical expressions for the end-to-end SNR derived in Section III will therefore start from photometric quantities, and we devise a simple method to convert them into corresponding radiometric quantities.

A particular strength of ReluxDesktop is that simulated illuminance values are highly accurate, as they are typically found within an uncertainty interval of $\pm 5\%$ around corresponding measurement results [31], [32]. Note that the uncertainty of measurements is usually on the same order. As will be seen in Section IV, this allows for accurate BER predictions for phosphorescent white-light LED-based lighting/VLC systems. In addition to [31], [32], we will present further accuracy results for ReluxDesktop in Section IV-F, which are based on a simulation technique employing a special LDC tailored to a particular 3D simulation setting under consideration.

III. SNR Prediction Based on 3D Light-Planning Simulations

In the following, we describe an end-to-end procedure to predict the available SNR at the assumed location of a VLC receiver based on a 3D light-planning simulation conducted with ReluxDesktop. Our procedure starts from simulated illuminance values "measured" at the location of the VLC receiver and involves several steps for converting photometric into radiometric quantities.

Inspecting Fig. 1, the SNR relevant for the resulting BER performance (associated with error events $\hat{\mathbf{u}} \neq \mathbf{u}$) is the average SNR in the *electrical* domain, which is defined as

$$\gamma_\mathrm{el} = \frac{P_\mathrm{R,el}}{N_\mathrm{R,el}}, \qquad (2)$$

where $P_\mathrm{R,el}$ denotes the average received power of the desired signal and $N_\mathrm{R,el}$ the average noise power at the receiver (both in the electrical domain).

A. Overall Average Received Power of the Desired Signal

The average received power $P_\mathrm{R,el}$ can directly be derived from the illuminance values E_V at the location of the assumed VLC receiver provided by the 3D light-planning simulation. As such, the test surface defined in ReluxDesktop should represent the assumed position, orientation, and size of the PD area of the VLC receiver. Note that the simulated illuminance values E_V include both the direct light signal from a VLC light source to the PD and possible multipath signal components reflected from walls or other objects within the simulation setting (including multiple reflections). Multiplying the illuminance E_V with the area of the PD yields the corresponding luminuous flux Φ_V. By definition, Φ_V refers to the radiation characteristics of the light source and is therefore associated with the VLC *transmitter* side. Correspondingly, a suitable test surface would naturally be defined as a sphere or partial sphere surface, whereas for the PD a plane test surface should be assumed (with area denoted as A_meas in the sequel). Yet, as long as the distance between the VLC light source and the PD of the assumed VLC receiver is sufficiently large, the curvature of the sphere surface is negligible. Therefore, we may write

$$\Phi_\mathrm{V} = E_\mathrm{V} \cdot A_\mathrm{meas} \qquad (3)$$

for the received luminuous flux. Note that Φ_V is a photometric quantity, which includes the eye sensitivity curve $V(\lambda)$ for human vision defined by the Commission Internationale de l'Eclairage (CIE) [4, Ch. 2.5], where λ denotes the wavelength of the emitted light. For the VLC part, however, radiometric quantities regarding received signal powers in Watt (W) are relevant, which requires a corresponding conversion. Inspecting the basic definition of the luminuous flux Φ_V,

$$\Phi_\mathrm{V} = 683 \frac{\mathrm{lm}}{\mathrm{W}} \int_{380\,\mathrm{nm}}^{780\,\mathrm{nm}} V(\lambda)\, \phi(\lambda)\, \mathrm{d}\lambda, \qquad (4)$$

where $\phi(\lambda)$ denotes the optical spectral power distribution (OSPD) in Watt per unit wavelength [4, Ch. 2.5], and comparing it to the basic definition of the radiated optical power,

$$P_\mathrm{T,opt} = \int_{380\,\mathrm{nm}}^{780\,\mathrm{nm}} \phi(\lambda)\, \mathrm{d}\lambda, \qquad (5)$$

it can be seen that a conversion from luminous flux to optical power is not straightforward for general wide-band light sources with arbitrary OSPD [33, Ch. 7]. A special case is a (quasi-) monochromatic light source with wavelength λ_0 and (effective) optical bandwidth B_opt. Assuming an ideal rectangular OSPD within the bandwidth B_opt, one obtains

$$\Phi_\mathrm{V} = 683 \frac{\mathrm{lm}}{\mathrm{W}}\, V(\lambda_0)\, \phi(\lambda_0)\, B_\mathrm{opt}$$

and

$$P_\mathrm{T,opt} = \phi(\lambda_0)\, B_\mathrm{opt},$$

which leads to the relation

$$P_\mathrm{T,opt} = \frac{\Phi_\mathrm{V}}{683 \frac{\mathrm{lm}}{\mathrm{W}} \cdot V(\lambda_0)}. \qquad (6)$$

Assuming a phosphorescent white-light LED and an ideal rectangular optical filter at the VLC receiver with center wavelength λ_b and optical bandwidth $B_\mathrm{opt,b}$ tailored to the blue core LED, we may reuse (6) with slight modifications to arrive at the optical

power at the receiver:

$$P_{\mathrm{R,opt}} = \frac{\xi \cdot \Phi_{\mathrm{V}}}{683\frac{\mathrm{lm}}{\mathrm{W}} \cdot V(\lambda_{\mathrm{b}})}. \tag{7}$$

Since in the ReluxDesktop simulation the illuminance values are measured at the VLC receiver, we have replaced $P_{\mathrm{T,opt}}$ by $P_{\mathrm{R,opt}}$. Moreover, $0 \leq \xi \leq 1$ denotes the effective fraction of the emitted optical power that falls within the passband of the optical receive filter, including also the transmittivity of the optical filter. The value of ξ needs to be calculated numerically for the particular light source under consideration, based on corresponding reference curves for the OSPD, which is usually included in the data sheet of the luminaire. Altogether, we may write

$$P_{\mathrm{R,opt}} = \frac{\xi \cdot E_{\mathrm{V}} \cdot A_{\mathrm{meas}}}{683\frac{\mathrm{lm}}{\mathrm{W}} \cdot V(\lambda_{\mathrm{b}})}. \tag{8}$$

Note that the assumption of ideal rectangular OSPDs and optical filters is an approximation justified by the relatively small optical bandwidth of practical LEDs. Furthermore, note that the angle of incidence does not need to be explicitly accounted for in (8), since it is already captured by the $\cos(\phi_{\mathrm{j}})$-term in (1). Correspondingly, it is included in the simulated E_{V}-value found on the right-hand side of (8).

A final aspect to take into account is the fact that state-of-art lighting systems are required to be energy-efficient and therefore need to be able to adapt their emitted light intensity to prevailing sunlight conditions, as discussed in the Introduction. To this end, we introduce a corresponding (optical) dimming parameter $0 \leq \delta \leq 1$, which leads to our final expression for the received optical power as a function of the simulated illuminance E_{V}:

$$P_{\mathrm{R,opt}}(E_{\mathrm{V}}) = \frac{\delta \cdot \xi \cdot A_{\mathrm{meas}}}{683\frac{\mathrm{lm}}{\mathrm{W}} \cdot V(\lambda_{\mathrm{b}})} \cdot E_{\mathrm{V}}. \tag{9}$$

Based on (9), the average received power of the desired signal in the electrical domain results as [4, Ch. 3.6]

$$P_{\mathrm{R,el}}(E_{\mathrm{V}}) = \kappa \cdot \left(\frac{R_{\lambda}(\lambda_{\mathrm{b}}) \cdot \delta \cdot \xi \cdot A_{\mathrm{meas}}}{683\frac{\mathrm{lm}}{\mathrm{W}} \cdot V(\lambda_{\mathrm{b}})} \cdot E_{\mathrm{V}} \right)^2, \tag{10}$$

where

$$\kappa := \frac{\mathrm{E}\{i_{\mathrm{PD}}^2(t)\}}{\mathrm{E}\{i_{\mathrm{PD}}(t)\}^2} \geq 1 \tag{11}$$

denotes the average-power-to-squared-mean ratio [47], which only depends on the properties of the modulated transmit signal $s(t)$ in Fig. 1 ($\mathrm{E}\{.\}$ denotes the expected value). For example, for non-return-to-zero (NRZ) OOK or PPM, a value of $\kappa = 2$ results. Furthermore, $R_{\lambda}(\lambda_{\mathrm{b}})$ denotes the responsivity of the PD for wavelength λ_{b} (in A/W), which is a device-dependent quantity.

Note that the simulated illuminance values E_{V} contain both the contribution of the direct LoS signal path and the indirect NLoS fraction, i.e., $E_{\mathrm{V}} = E_{\mathrm{V,LoS}} + E_{\mathrm{V,NLoS}}$. ReluxDesktop allows to separate both contributions by simulating only the direct fraction. Yet, as ReluxDesktop is tailored to unmodulated light signals, the NLoS fraction needs to be weighted with a factor $\psi_{\mathrm{NLoS}} \leq 1$, which accounts for the low-pass behavior of the NLoS component of VLC channels. This depends on the geometry of the room and the considered (electrical) signal bandwidth, which will be discussed in Section IV-C.

B. Average Noise Power at the VLC Receiver

Due to the assumed mixing step within the transmitter driver circuit and the corresponding BPF at the receiver, direct interference effects due to ambient (unmodulated) light sources may be disregarded. Still, ambient light causes an increased noise level due to generated shot noise. Correspondingly, the average noise power at the VLC receiver in the electrical domain can be written as [34]

$$N_{\mathrm{R,el}} = N_{\mathrm{shot}} + N_{\mathrm{th}}. \tag{12}$$

Here,

$$N_{\mathrm{shot}} := 2\, e_0\, R_{\lambda}(\lambda_{\mathrm{b}})\, P_{\mathrm{R,amb}}\, B_{\mathrm{MF}} \tag{13}$$

denotes the average shot noise power, $P_{\mathrm{R,amb}}$ the accumulated average optical power of ambient light sources at the position of the VLC receiver, and $e_0 := 1.602 \cdot 10^{-19}$ As denotes the elementary charge. (Note that the matched-filter bandwidth B_{MF} rather than the bandwidth $B_{\mathrm{filt,el}}$ of the electrical BPF is the relevant quantity here, since $B_{\mathrm{MF}} \leq B_{\mathrm{filt,el}}$, cf. Section II-A.) Moreover,

$$N_{\mathrm{th}} \approx 4\, k_{\mathrm{B}}\, T_{\mathrm{a}}\, B_{\mathrm{MF}}/R_{\mathrm{F}} \tag{14}$$

denotes the average thermal noise power, where $k_{\mathrm{B}} = 1.38 \cdot 10^{-23}$ Ws/K is the Boltzmann constant, T_{a} is the absolute temperature in K, and R_{F} denotes the feedback resistor of the TIA (in Ω).

In the ReluxDesktop simulation suite, various ambient light sources can be included in the simulation as desired, including sunlight and several types of artificial light sources. The accumulated average optical power $P_{\mathrm{R,amb}}$ due to ambient light can then be assessed in the ReluxDesktop simulation by disabling the VLC light source and successively activating the L_{amb} ambient light sources. By this means, one obtains

$$P_{\mathrm{R,amb}} = \frac{A_{\mathrm{meas}}}{683\frac{\mathrm{lm}}{\mathrm{W}} \cdot V(\lambda_{\mathrm{b}})} \cdot \sum_{k=1}^{L_{\mathrm{amb}}} \tilde{\xi}_k \cdot \tilde{E}_{\mathrm{V},k}, \tag{15}$$

where $\tilde{E}_{\mathrm{V},k}$ denotes the illuminance value measured for the kth light source and $0 \leq \tilde{\xi}_k \leq 1$ the corresponding effective fraction of the optical power that falls within the passband of the optical receive filter (including the transmittivity of the optical filter). Note that saturation effects in the electrical domain have not been taken into account.

IV. BER Prediction for Basic Office Scenarios and Numerical Evaluation

Based on the method described in Section III, some basic office scenarios are evaluated in the sequel. The final objective is to arrive at BER predictions for (single-carrier) OOK and M-ary PPM schemes, while taking real-world luminaires (with corresponding LDCs), multipath signal propagation (including

multiple reflections), ambient light as well as options for adaptive dimming operations into account. First, we briefly discuss the basic office setups and parameter settings used for our ReluxDesktop simulations. Then, we devise a general framework incorporating dimming operations for two different cases. Based on this framework, we then conduct numerical evaluations of the overall average SNR γ_{el} in the electrical domain for selected examples, where we study both line-of-sight (LoS) and NLoS conditions. To this end, we inspect corresponding analytical BER results that are valid for propagation scenarios without any ISI effects. As will be discussed in Section IV-C, this is justified when assuming a realistic electrical bandwidth of the blue core LED ($B_{\mathrm{LED,el}} \leq 20$ MHz). We conclude the section with a discussion on the resulting accuracy of our BER predictions that is achieved based on ReluxDesktop simulations.

A. Settings for ReluxDesktop Simulations

As an exemplary scenario, a room with a base area of 5 m $\times$ 5 m and a height of 3 m is set up in ReluxDesktop. The workflow for planning a joint lighting/VLC system would be as follows: The given setting would first be optimized by a light planner, by placing office desks and other furniture within the simulation setup and varying the locations of luminaires accordingly – with the final goal to meet requirements regarding workspace ergonomics and to create a favorable overall light atmosphere. Once the simulation setting is finalized, SNR and BER predictions could then be conducted for the VLC part, by evaluating selected locations of the assumed PD.

Throughout the ReluxDesktop simulations, the radiosity computation kernel is employed using the "high indirect fraction" simulation mode. To provide a simple benchmark case within the scope of this paper, we consider a basic setup with a single office desk and a single luminaire – assuming a VLC-enabled phosphorescent white-light LED. Corresponding three-dimensional and layout views exported from the ReluxDesktop simulation suite are shown in Fig. 2. The reflection coefficients of surfaces can be freely chosen in the simulation suite and are set to 0.5 for the walls, 0.7 for the ceiling, 0.2 for the floor, and 0.4 for the door, which is placed at wall #1 (W1). The surface parameters were chosen along the lines of [20], [26]. For all simulations presented in the sequel, the order of reflections taken into account is adjusted dynamically, such that the simulation accuracies reported in Section IV-F are attained. Within the simulation scenario, the luminaire is placed at the ceiling, centered above the office desk. For the office desk a customary height of 0.75 m is chosen. In the baseline scenario ("Scenario 1"), the center point of the luminaire is given by $(x, y) = (2.50\ \mathrm{m}, 2.50\ \mathrm{m})$, where the reference point $(x, y) = (0\ \mathrm{m}, 0\ \mathrm{m})$ is found at the intersection of wall #1 and wall #4, cf. Fig. 2. The layout view at the bottom of Fig. 2 shows the exemplary location of the test surface (M1), which is placed in the center of the office desk right underneath the luminaire. The area of the test surface M1 represents the PD area of the assumed VLC receiver and is chosen as 100 mm^2 (in accordance to the Hamamatsu S3590-08 PIN photodiode [35]). Furthermore, a window of size 1.50 m $\times$ 1.50 m with a transmittivity value of 0.9 is placed within the eastern wall #2 with center point at $(x, y) = (5.00\ \mathrm{m}, 2.50\mathrm{m})$ and height 1.65 m, allowing sunlight into the room simulated according to the CIE "clear sky with sun" specifications [36], tailored to the location of Hamburg and the date June 21. Further sources of ambient light are not taken into account for simplicity ($L_{\mathrm{amb}} = 1$).

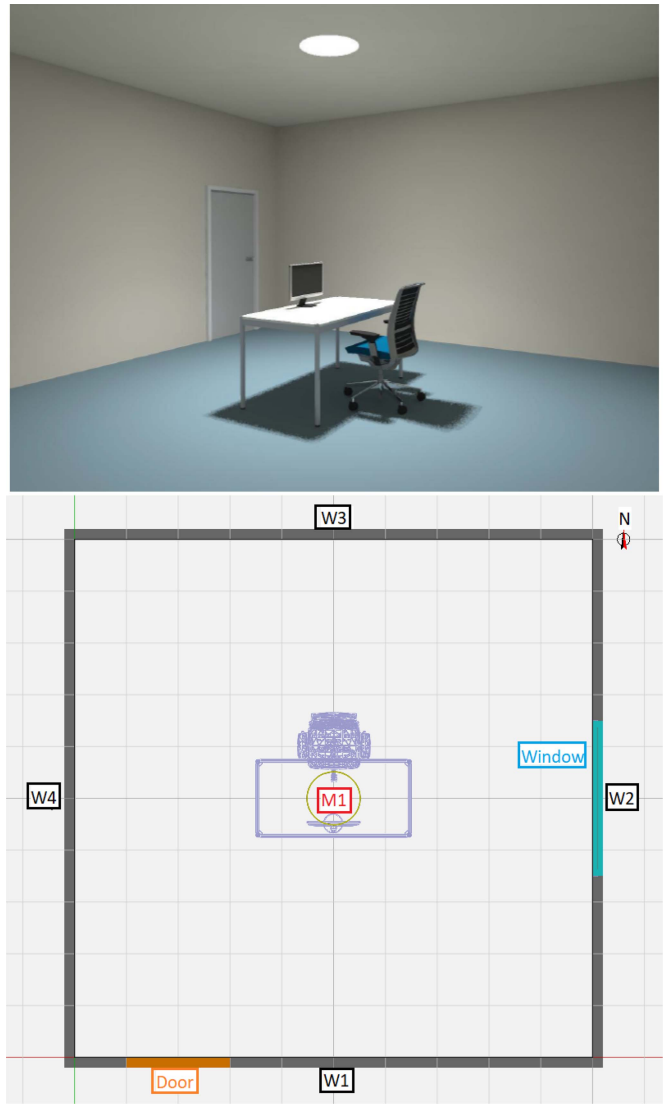

Fig. 2. Views of the considered ReluxDesktop simulation scenario – a three-dimensional view (top) and a layout view (bottom) showing the location of the test surface (M1) placed in the center of the office desk. The test surface represents the PD area of the assumed VLC receiver.

As an example, two different luminaire types from the ReluxDesktop data base are considered, which are typical for office environments, namely

1) Regent Solo Slim (luminuous flux $\Phi_{\mathrm{V}} = 4350$ lm),
2) Philips Maxos LED (luminuous flux $\Phi_{\mathrm{V}} = 6600$ lm).

The corresponding LDCs in candela (cd) per 1000 lm are shown in Fig. 3 . While the LDC for the Solo Slim luminaire is rotationally symmetric, the LDC for the Maxos LED is different for the xz-plane (C0) and the yz-plane (C90), where z denotes the vertical dimension.

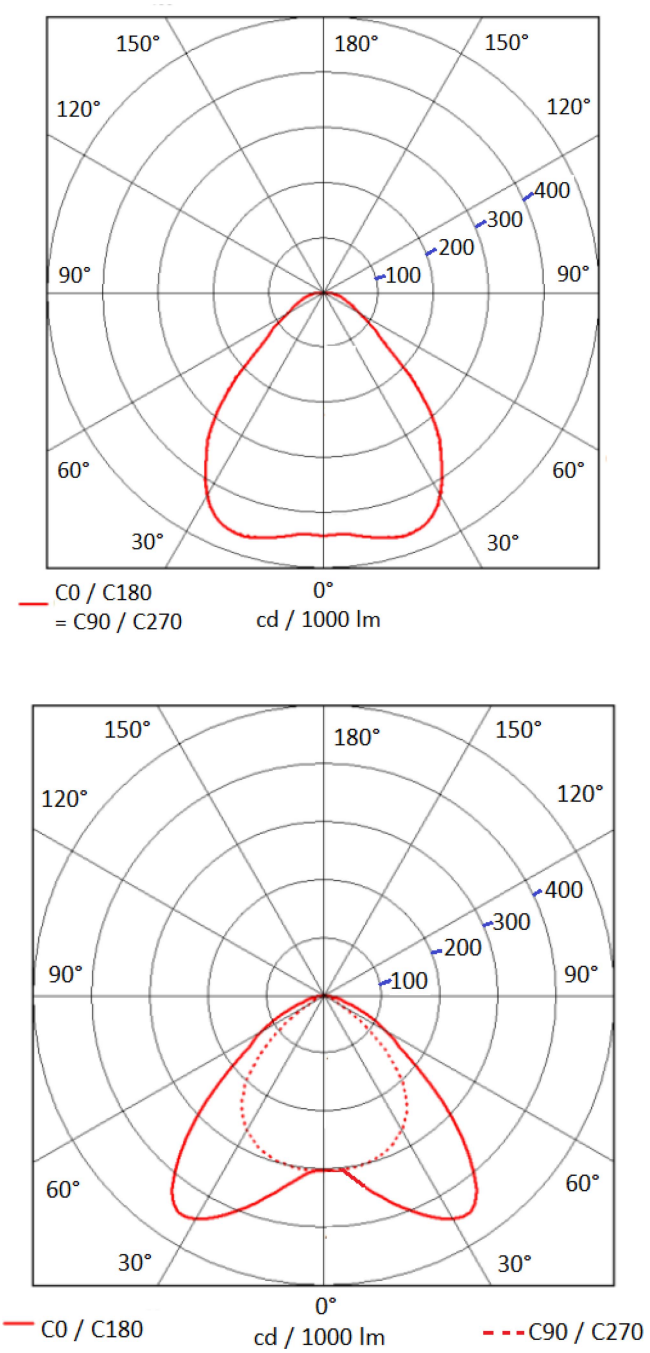

Fig. 3. LDCs of the considered luminaires – Regent Solo Slim (top) and Philips Maxos LED (bottom).

In addition to the benchmark scenario ("Scenario 1"), two alternative geometrical settings are considered, in order to study different multipath signal propagation conditions. Referring to the center-point position of the luminaire, these are defined as follows:

1) Scenario 1: $(x, y) = (2.50\text{ m}, 2.50\text{ m})$,
2) Scenario 2: $(x, y) = (4.00\text{ m}, 2.50\text{ m})$,
3) Scenario 3: $(x, y) = (4.00\text{ m}, 4.00\text{ m})$.

For all simulation scenarios, the center point of the office desk and the test surface is kept in line with the center point of the luminaire.

In the following, we assume that the modeled room is equipped with an (automatic) lighting system able to respond to prevalent sunlight conditions by means of adaptive dimming. To this end, optical dimming factors $\delta \leq 1$ are taken into account in the sequel.

B. Analytical BER Expressions Incorporating Dimming

In the following, it is assumed that dimming is accomplished either (i) by adjusting the duty cycle of the transmitted OOK or PPM signals or (ii) by adjusting the supply current of the VLC-enabled LED. Alternatively, suitable compensation times could be used, in order to accomplish a desired (average) brightness level [37]. For dimming case (i), the pulse length – denoted as T in the sequel – is adjusted proportionally to the desired optical dimming factor δ, according to

$$T = \delta \cdot T_0, \tag{16}$$

where T_0 denotes the nominal pulse length for maximum light intensity [4, Ch. 4.3]. For OOK, the maximum duty cycle (corresponding to $\delta = 1$) is equal to one (NRZ signal format), whereas for M-ary PPM the maximum duty cycle is assumed to be $1/M$ in the sequel. Correspondingly, for $\delta < 1$ one obtains a return-to-zero (RZ) OOK or a variable PPM (VPPM) scheme, respectively. Note that the analog BPF at the receiver (in the electrical domain) will be tailored to the minimum pulse length $T_{\min}$ associated with the minimum dimming level $\delta_{\min}$, according to $B_{\text{filt,el}} \approx 1/T_{\min}$, whereas the (digital) matched filter should be matched to the actual pulse length T, i.e., $B_{\text{MF}} \approx 1/T \leq B_{\text{filt,el}}$. In other words, the adjusted dimming factor δ must be known at the receiver and either needs to be measured at the receiver side or conveyed by the transmitter as side information. For dimming case (ii), on the other hand, the OOK/PPM scheme always operates with the nominal pulse length $T = T_0$, so that $B_{\text{MF}} \approx 1/T = 1/T_0 \approx B_{\text{filt,el}}$ can be assumed, and no knowledge of the adjusted dimming factor δ at the receiver is required. Note that the relation $P_{\text{T,opt}} = f(i_{\text{F}}(t))$ between the output current $i_{\text{F}}(t)$ of the transmit driver and the resulting optical power $P_{\text{T,opt}}$ is in general non-linear [38]. However, this aspect is not relevant here, since we consider *optical* dimming factors throughout. Yet, for a desired optical dimming factor δ (and corresponding optical power $P_{\text{T,opt}}$), the output current $i_{\text{F}}(t)$ of the transmit driver needs to be adjusted according to the inverse relation $i_{\text{F}}(t) = f^{-1}(P_{\text{T,opt}})$, using a calibrated current control loop.

The analytical bit error probability (BEP) for NRZ-OOK in the absence of ISI effects is given by [4, Ch. 4.3]

$$P_{\text{b}} = \text{Q}(\sqrt{\gamma_{\text{s}}}), \tag{17}$$

where

$$\gamma_{\text{s}} := B_{\text{MF}} \cdot T \cdot \gamma_{\text{el}} \tag{18}$$

denotes the average SNR per data symbol (in the electrical domain) and

$$\text{Q}(x) := \frac{1}{\sqrt{2\pi}} \int_x^\infty \text{e}^{-\tau^2/2}\,\text{d}\tau \tag{19}$$

denotes the Gaussian Q-function. It is related to the complementary error function according to $\text{Q}(x) = 0.5 \cdot \text{erfc}(x/\sqrt{2})$. In the

following, we assume $B_{\mathrm{MF}} = 1/T$ for simplicity, i.e., $\gamma_{\mathrm{s}} = \gamma_{\mathrm{el}}$. In the case of dimming, the BEP expression for NRZ-OOK is still valid, as the optical dimming factor $\delta < 1$ is incorporated in the SNR γ_{el}, cf. Section III-A.

Similarly, for M-ary (V)PPM with maximum duty cycle $1/M$, the analytical BEP for equal energy orthogonal signals can be adopted, which is given by [39, Ch. 4.4]

$$P_{\mathrm{b}} = \frac{M}{2(M-1)} \frac{1}{\sqrt{2\pi}} \int_{-\infty}^{+\infty} \left[1 - (1 - \mathrm{Q}(z))^{M-1}\right] \times \times \exp\left[-\frac{\left(z - \sqrt{2\gamma_{\mathrm{s}}}\right)^2}{2}\right] \mathrm{d}z. \tag{20}$$

The integral expression in (20) needs to be evaluated by means of numerical integration. Note that under dimming case (i), a dimming factor of $\delta = 1$ means that the considered VPPM scheme operates with the nominal pulse length T_0, corresponding to the maximum duty cycle. Generally, in the absence of dimming, the different (V)PPM schemes are all normalized to an average received energy of one, which means that transmitted pulses are scaled with an amplitude of $\sqrt{M}$ (in the electrical domain). Correspondingly, dimming can be applied on top, and a fair comparison between modulation schemes with different cardinality M is possible. As for OOK, the optical dimming factor $\delta < 1$ is incorporated in the SNR $\gamma_{\mathrm{s}} = \gamma_{\mathrm{el}}$, as discussed in Section III-A.

In particular, the average received power in the electrical domain, $P_{\mathrm{R,el}}(E_{\mathrm{V}})$, scales with δ^2 (cf. (10)). Moreover, when dimming is realized by adjusting the duty cycle of the transmitted OOK or PPM signals (dimming case (i)), the bandwidth of the matched filter, B_{MF}, scales with $1/T = 1/(\delta \cdot T_0)$. Correspondingly, the average SNR per data symbol scales as

$$\gamma_{\mathrm{s}} = \gamma_{\mathrm{s},0} \cdot \delta^3 \tag{21}$$

in this case, where $\gamma_{\mathrm{s},0}$ denotes the reference value for maximum light intensity (pulse length T_0). However, when dimming is realized by adjusting the supply current of the LED (dimming case (ii)), the bandwidth of the matched filter is constant ($B_{\mathrm{MF}} = 1/T_0$), and the average SNR per data symbol scales as

$$\gamma_{\mathrm{s}} = \gamma_{\mathrm{s},0} \cdot \delta^2. \tag{22}$$

Generally, in practice a wide range of dimming factors is desirable – mainly depending on prevalent sun light conditions (related to adaptive dimming systems) and user preferences. For unmodulated light sources, very high contrast ratios are possible, e.g., up to 3000:1. A duty cycle of one is possible in the limit. With data transmission, the dimming factor is limited – typically between $0.1 \leq \delta \leq 0.9$, when adjusted via the pulse length (dimming case (i)) [9]. With current control (dimming case (ii)), however, a significantly wider range of contrast ratios is achievable. Note that the optical dimming factor δ may be relatively small, as the light intensity perceived by humans is associated with the square-root of δ [40, Ch. 27]. Therefore, for $\delta = 0.01$ the perceived light intensity still results as 10%.

While an advanced lighting concept should take material properties into account – such as the color or the absorption coefficients of walls, furniture surfaces, and the flooring – this will mainly affect the choice of the luminaire, regarding its radiated optical power or OSPD. Simulations in ReluxDesktop can assist the light planning process by offering both qualitative results (in terms of 3D visual impressions) and quantitative results (in terms of simulated illuminance values). However, the dimming factor δ is associated with *dynamic* adjustments of light intensities, e.g., in response to changing ambient light conditions. Correspondingly, for BER predictions, simulations in ReluxDesktop should be conducted employing the nominal optical power of the selected luminaire, and dimming factors should be incorporated via (21)/(22), depending on the underlying dimming case (i)/(ii), respectively.

C. Parameter Settings and Simulation Results From ReluxDesktop

In the following, the underlying system parameters are summarized which are adopted throughout for evaluating the average SNR γ_{el} in the electrical domain, cf. (2), (10) and (12)–(14):

- The average-power-to-squared-mean ratio is set to $\kappa = 2$ both for (NRZ) OOK and M-ary (V)PPM. In the sequel, rectangular pulse shapes are assumed throughout, i.e. the corresponding matched filter reduces to the well-known integrate-and-dump receiver.
- For the blue core LED, a center wavelength of $\lambda_{\mathrm{b}} = 450\,\mathrm{nm}$ is assumed. The corresponding value of the eye sensitivity curve is given by $V(\lambda_{\mathrm{b}}) = 0.04$.
- For the responsivity of the PD at this wavelength, a value of $R_\lambda(\lambda_{\mathrm{b}}) = 0.28$ A/W is adopted from the data sheet of the Hamamatsu S3590-08 PIN photodiode [35].
- The passband of the corresponding optical filter at the receiver is assumed to be found between $\lambda = 430$ nm – 470 nm, which has been adopted from the data sheet of the Royal Blue LUXEON Rebel filter [41] (tailored to the center wavelength of the blue core LED).
- For the effective fraction of the emitted optical power that falls within the passband of the optical filter, a value of 0.166 has been calculated for the Solo Slim luminaire, based on an internal measurement report provided by Regent Lighting. For the Philips Maxos LED luminaire, a corresponding value of 0.116 has been acquired based on own measurements of the OSPD. For the sunlight, an OSPD according to the CIE standard illuminant model D65 has been assumed [42, Ch. 3], which leads to a value of 0.120. Assuming a transmittivity value of 0.9 for the optical filter, one obtains values of $\xi = 0.149$ for the Solo Slim luminaire, $\xi = 0.104$ for the Maxos LED luminaire, and $\tilde{\xi} = 0.108$ for the sunlight.
- The area of the test surface representing the VLC receiver is given by $A_{\mathrm{meas}} = 100\ \mathrm{mm}^2$ [35], cf. Section IV-A.
- For the absolute temperature, a value of $T_{\mathrm{a}} = 293.15$ K is assumed.
- For the feedback resistor of the TIA, a value of $R_{\mathrm{F}} = 10\,\mathrm{k}\Omega$ is assumed.
- The LDCs of the considered luminaires, cf. Fig 3, were directly incorporated into the ReluxDesktop simulation.

From the ReluxDesktop simulations, the following values for the illuminance E_{V} across the test surface M1 are obtained for the Regent Solo Slim luminaire: Scenario 1 – $E_{\mathrm{V}}=319.1$ lx ($\Delta=0.1$ lx), Scenario 2 – $E_{\mathrm{V}}=328.1$ lx ($\Delta=0.4$ lx), Scenario 3 – $E_{\mathrm{V}}=357.7$ lx ($\Delta=0.2$ lx), which illustrates the growing fraction of NLoS signal components, as the luminaire is placed closer to the eastern wall #2. The stated illuminance values E_{V} are averaged across the area of the test surface M1, while the Δ-values represent the corresponding maximum positive or negative deviation. In the sequel, the average illuminance values are employed for assessing the electrical SNR γ_{el} at the receiver. The corresponding (average) illuminance values associated with the combined NLoS signal components are given by 15.3 lx, 24.3 lx, and 53.9 lx for Scenario 1–3, respectively. For the Philips Maxos LED luminaire, an illuminance value of $E_{\mathrm{V}}=357,0$ lx ($\Delta=0.1$ lx) results for Scenario 1, while the fraction associated with the combined NLoS signal components is given by 21.5 lx. Furthermore, for the simulated sunlight the following illuminance values are obtained: Scenario 1 – $\tilde{E}_{\mathrm{V}}=675.4$ lx ($\Delta=2.2$ lx), Scenario 2 – $\tilde{E}_{\mathrm{V}}=1792.9$ lx ($\Delta=6.3$ lx), Scenario 3 – $\tilde{E}_{\mathrm{V}}=569.3$ lx ($\Delta=19.8$ lx).

In accordance with the typical electrical bandwidth offered by the blue core LED, we consider a realistic baud rate of 20 MSymbol/s for the OOK and PPM schemes in the sequel and assume a matched filter bandwidth of $B_{\mathrm{MF}}=20$ MHz, which – under dimming case (i) – holds for the maximum duty cycle, cf. Section IV-B, while for dimming case (ii) it is a fixed parameter. Additional BER simulations – not included for the sake of conciseness – incorporating (approximate) power delay profiles, rectangular pulses, and a matched-filter step realized by an integrate-and-dump receiver, have shown that ISI effects can safely be neglected for the room geometry and the moderate baud rates under consideration. This is also in accordance with the findings in [25], where ISI effect are only associated with data rates in the Gb/s regime. Correspondingly, we will employ the analytical BER expressions from Section IV-B disregarding any ISI effects. Note, however, that OWC channels are usually characterized by a distinct low-pass behavior affecting the NLoS fraction generated by multiple signal reflections [18], [43], [44]. For the room dimensions considered within the scope of this paper, a 3-dB bandwidth of 6 MHz can be assumed. Corresponding, the NLoS fraction $E_{\mathrm{V,NLoS}}$ of E_{V} is scaled with a factor of $\psi_{\mathrm{NLoS}}=0.3$ in the sequel, as the ReluxDesktop simulations are tailored to unmodulated light signals.

D. BER Prediction for LoS Conditions

Given the system parameters listed above, resulting analytical BEP curves for OOK and (V)PPM are shown in Figs. 4– 7 (solid lines), considering the two different dimming cases outlined in Section IV-B. For OOK, when dimming is accomplished by adjusting the duty cycle of the transmitted pulse sequence (Fig. 4), low BEP values ($\leq 10^{-6}$) are attained for dimming factors of $\delta \geq 0.02$ for all considered scenarios, corresponding to a minimum perceived light intensity of 14.1 %. However, when dimming is performed by adjusting the supply current of the LED (Fig. 5), even smaller dimming factors $\delta \geq 0.003$ are feasible (corresponding to a minimum perceived light intensity of 5.5 %), since the average SNR per data symbol, γ_{s}, scales only with δ^2 instead with δ^3, cf. (21), (22). Corresponding analytical BEP curves for (V)PPM under the two dimming cases are presented in Figs. 6 and 7, respectively. Altogether, similar results are obtained as for OOK, while an increase of the modulation cardinality to $M=64$ leads to moderate performance degradations. Hence, (V)PPM is an attractive means to increase the data rate by a factor of $\log_2(M)$ compared to the baud rate $1/T$.

For the LoS case, the direct path is clearly dominant (cf. Section IV-C). Since the luminaire and the PD are kept in line when being moved towards the window and the surrounding walls (Scenario 1 to 3), the contribution of the LoS component

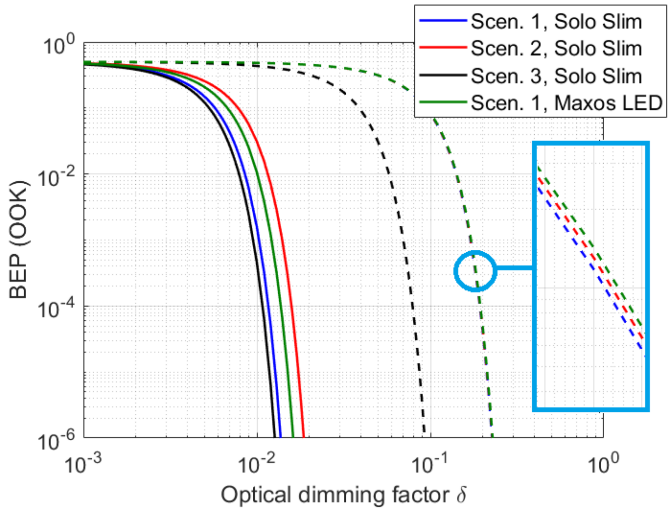

Fig. 4. Analytical BEPs for OOK under Scenario 1 – 3 and dimming case (i), where the duty cycle of the transmitted pulse sequence is adjusted. Solid lines: LoS operation; dashed lines: Non-LoS operation.

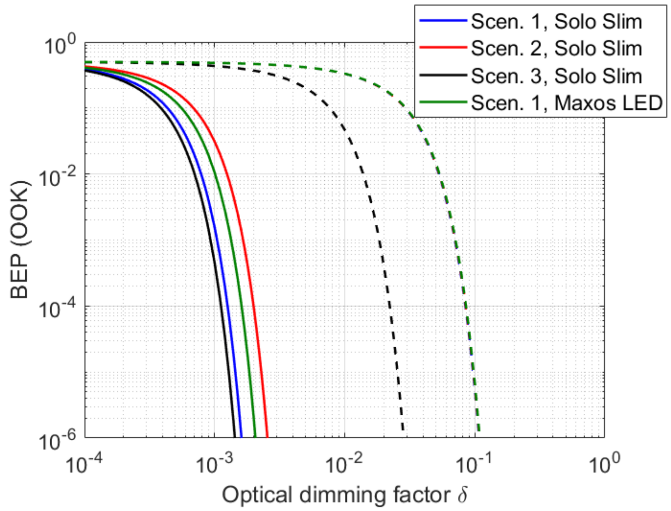

Fig. 5. Analytical BEPs for OOK under Scenario 1 – 3 and dimming case (ii), where the supply current of the LED is adjusted. Solid lines: LoS operation; dashed lines: Non-LoS operation.

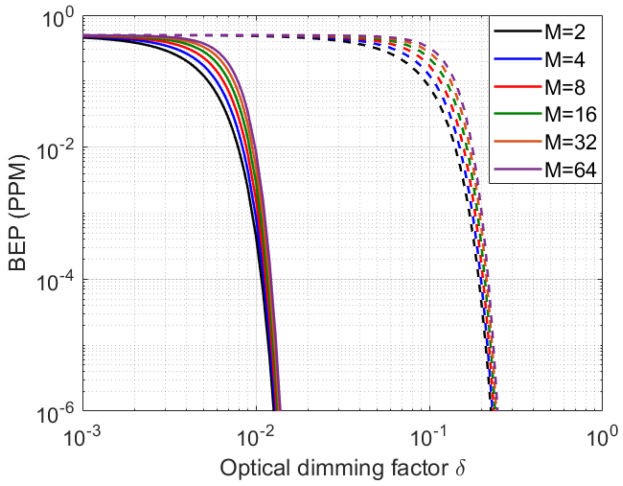

Fig. 6. Analytical BEPs for M-ary VPPM for different cardinalities M under dimming case (i), where the duty cycle of the transmitted pulse sequence is adjusted. Solid lines: LoS operation (Scenario 3, Solo Slim luminaire); dashed lines: Non-LoS operation (Scenario 1, Solo Slim luminaire).

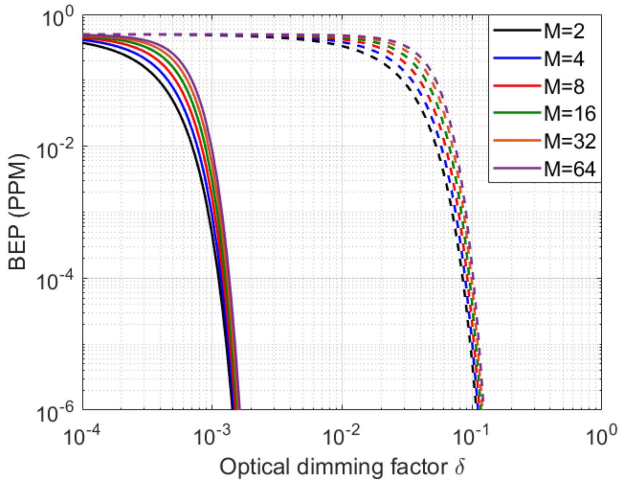

Fig. 7. Analytical BEPs for M-ary PPM for different cardinalities M under dimming case (ii), where the supply current of the LED is adjusted. Solid lines: LoS operation (Scenario 3, Solo Slim luminaire); dashed lines: Non-LoS operation (Scenario 1, Solo Slim luminaire).

stays the same in all considered scenarios. Scenario 1 leads to a superior BEP compared to Scenario 2, since the influence of the direct sunlight (and thus the resulting shot noise level) is significantly smaller, due to a larger distance to the window. Scenario 3 also leads to a superior BEP compared to Scenario 2 (and even compared to Scenario 1), since the (horizontal) incidence direction of the sunlight is no longer perpendicular w.r.t. the PD area, which leads to a reduction of illuminance values according to a cosine law, cf. (1). The influence from changing the luminaire can be seen when comparing the BEP curves for OOK in Scenario 1. Despite providing a smaller luminous flux, the BEP for a VLC-enabled Regent Solo Slim luminaire is slightly superior compared to the Philips Maxos LED. This is due to the fact that the LCD of the Solo Slim luminaire is characterized by a larger value in the direction of the PD, which is 0° in this setting (cf. Fig. 3). For all scenarios, it is found that the average power of the thermal noise is much smaller than the average power of the shot noise generated by the impinging sunlight ($N_{\mathrm{th}} \ll N_{\mathrm{shot}}$).

E. BER Prediction for NLoS Conditions

In practice, it may happen that the LoS path is (temporally) blocked, for example because the user accidentally places an object or his/her hand or arm in between the luminaire and the PD area of the VLC receiver. It is therefore interesting to evaluate, whether and for which dimming factors VLC might still work under NLoS conditions.

In the following, we assume that the NLoS signal components still reach the PD, while the LoS signal component is completely blocked. Based on the simulated illuminance values for the NLoS signal components stated in Section IV-C, corresponding BEP results have been included in Figs. 4–7 (dashed lines). As can be seen, low BEP values ($\leq 10^{-6}$) can still be attained, however, only for dimming factors of $\delta \geq 0.22$ for dimming case (i) and $\delta \geq 0.1$ for dimming case (ii), corresponding to minimum perceived light intensities of 46.9 % and 31.6 %, respectively. Therefore, for the considered scenarios the VLC link may theoretically still be maintained based on the received signal energy offered by the NLoS signal components, provided that the perceived light intensity is not dimmed by more than 50 %.

As can be seen in Figs. 4 and 5, the BER curves for Scenario 1,2 – employing the Regent Solo Slim luminaire – and Scenario 1 – employing the Philips Maxos LED – are very similar for both dimming cases (refer to Fig. 4 for an enlarged section of the BEP plot). Without dimming, the resulting SNR values are given by 32.86 dB, 32.81 dB, and 32.77 dB, respectively. Obviously, for the NLoS case the different LDCs associated with Scenario 1 do not play a significant role. Comparing Scenario 1 and 2, both the luminaire and the PD are moved towards the window (along a centered line), so that the contributions of the reflected NLoS components and the sunlight are increased to a similar extent, keeping the SNR basically unchanged. In Scenario 3, however, the contribution of the reflected NLoS components is further increased, due to a closer proximity to the walls, while the contribution of the sunlight is reduced significantly, due to the change in geometry (cf. Section IV-D). This leads to a notable improvement of the BEP curve for both dimming scenarios in Figs. 4 and 5.

F. Accuracy of Light-Planning Simulations

The accuracy of the underlying light-planning simulations is crucial with regard to the quality of corresponding BER predictions. Extensive analyses for ReluxDesktop have shown that simulated illuminance values are typically found within an uncertainty interval of $\pm 5\%$ around corresponding measurement results [31], [32]. In particular, simulation results of ReluxDesktop were validated against experimental reference data for different CIE test cases. In fact, an uncertainty interval of $\pm 5\%$ allows accurate BER predictions, as illustrated in Fig. 8, where analytical BEPs for OOK and PPM (with cardinality $M = 64$)

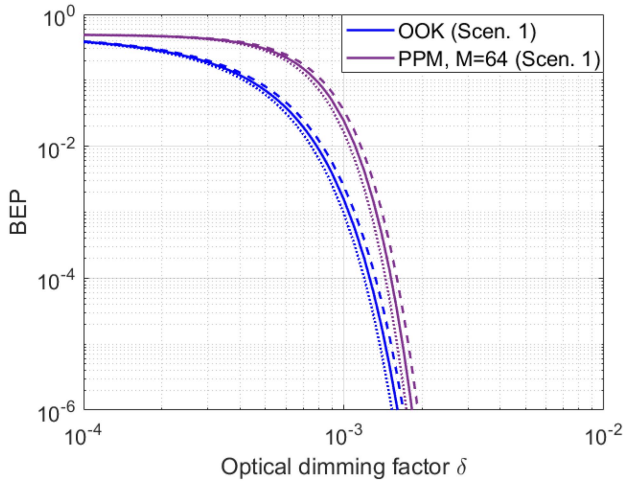

Fig. 8. Analytical BEPs for OOK and PPM ($M = 64$) for Scenario 1 (Solo Slim luminaire) under dimming case (ii), where the supply current of the LED is adjusted. Solid lines: Simulated illuminance values; dashed lines: Deviation from simulated illuminance values by -5%; dotted lines: Deviation from simulated illuminance values by $+5\%$.

are shown for Scenario 1 (Solo Slim luminaire) under dimming case (ii). Solid lines represent the corresponding BEP results employing the simulated illuminance values from Section IV-C, as presented in Figs. 5 and 7. Furthermore, alternative BER predictions are included, which would result if the simulated illuminance value deviated by -5% (dashed lines) or $+5\%$ (dotted lines). As can be seen, the three predicted BER curves are relatively close to each other, both for OOK and for PPM. In particular, the resulting uncertainty regarding the feasible dimming factor is rather small. Corresponding simulation results for dimming case (i) – not included for the sake of conciseness – are very similar.

The results in [31], [32] can be further corroborated by means of an *intrinsic* accuracy analysis, which is solely based on corresponding test simulations within ReluxDesktop. To this end, for a given 3D room geometry and luminaire position of interest, an LDC is calculated based on physical optics, which – theoretically – produces uniform illuminance values across all surfaces within the room, particularly across the entire walls and the floor surface. A corresponding software tool for calculating the test LDC is provided by the German Association of Light Technology (LiTG) [45]. Fig. 9 illustrates the test LDC which results for the basic setting in Scenario 1. The calculated LDC can then be imported to ReluxDesktop, and the variation of the simulated illuminance values across the walls and the floor surface can be assessed accordingly. For the basic setting under consideration – which serves well as a reference case – standard deviations of $11.8...11.9$ lx were observed for the illuminance values across the four walls (assessed over 260 measurement points per wall), while for the floor surface a standard deviation of 10.2 lx was assessed (over 400 measurement points). These values correspond to deviations of $\pm$ 3.3...3.4% for the walls and $\pm$ 3.0 % for the floor, which matches well with the accuracy results reported in [31], [32]. Therefore, the BER deviations shown in Fig. 9 seem to be a good representation.

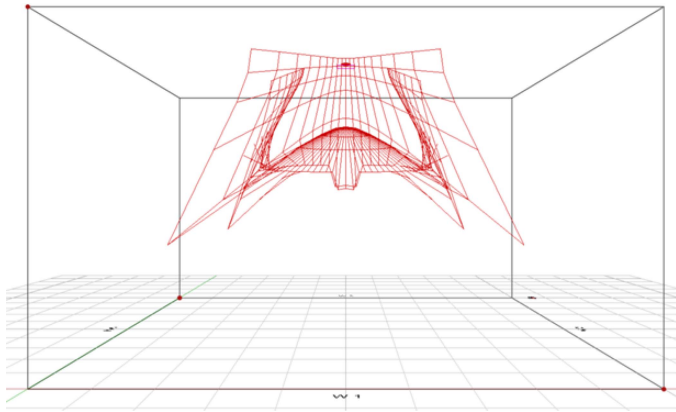

Fig. 9. Test LDC for the basic setting in Scenario 1 for the intrinsic accuracy analysis of ReluxDesktop light planning simulations.

V. Conclusion

We have addressed error-rate prediction for dual-use lighting systems with VLC functionality and have devised methodologies, how realistic receiver SNRs and corresponding end-to-end BERs can be predicted as a by-product extracted from advanced 3D light-planning simulation models. As a result, our BER predictions may be tailored to particular office settings, exemplary positions of a VLC receiver, and specific light plans of interest – and may start, as soon as the light design phase regarding the illumination part has been finalized (captured in a final simulation model). In particular, realistic LDCs of luminaires, multipath signal propagation as well as sources of ambient light are included in the 3D light-planning simulation model, while (automatic) dimming operations may be incorporated based on our presented SNR analysis. As our focus was on high-quality dual-use lighting/VLC systems employing phosphorescent white-light LEDs, we found that ISI effects can basically be neglected for the considered scenarios, single-carrier modulation schemes, and practicable electrical bandwidths.

In order to provide some simple benchmark cases, a basic office setup was simulated with ReluxDesktop. For the considered scenarios, it was found that LoS operation is theoretically possible for rather small dimming factors (for example $\delta = 0.02$ or smaller, depending on the employed modulation scheme and dimming technique). When planning dual-use lighting/VLC systems with automatic dimming function, it is therefore important to define a suitable lower brightness limit, in order to enable continuous operation of the VLC part. Furthermore, it was found that VLC links may even be maintained under NLoS operation, provided that only marginal dimming is applied – which may increase user acceptance.

Furthermore, we have shown that based on simulation results obtained with ReluxDesktop, accurate SNR predictions are possible. Given a known relation between the SNR and the resulting BEP – which was exemplified for OOK and (V)PPM – our work thus enables corresponding accurate BER predictions.

For future work, it will be of interest to investigate more complex modulation schemes, in particular relevant multi-carrier

schemes, such as optical orthogonal frequency-division multiplexing (OFDM) – possibly, including water-filling at the transmitter side, and to simulate more complex office scenarios or even more general use cases. In particular, it will be interesting to visualize corresponding coverage maps of acceptable BERs for complex scenarios and to verify predicted coverage areas against measurements with practical VLC systems. To this end, an accurate model of the measurement environment in ReluxDesktop will be required. Furthermore, an extension of the presented methodology to wide-band light sources with arbitrary OSPD and/or larger electrical bandwidths will be of interest. This will also entail the incorporation of ISI effects in our BER predictions. Finally, since our presented framework is based upon simulated illuminance values, from which we deduce SNR values at the receiver (in the optical and in the electrical domain), it is in principle also suited for investigating future hybrid classical/quantum schemes for VLC, such as the one investigated in [46] for an outdoor free-space optical link (although atmospheric effects are currently not included in ReluxDesktop).

Acknowledgment

Many thanks to Prof. Dr. Henrik Schulze (South Westphalia University of Applied Sciences, Germany) for fruitful discussions regarding simulation methods for indoor OWC channels. Furthermore, the authors also would like to thank Regent Lighting for providing a measurement report for the Solo Slim luminaire. Finally, we acknowledge support for the article processing charge by the Open Access Publication Fund of Hamburg University of Applied Sciences.

References

[1] S. Dimitrov and H. Haas, *Principles of LED Light Communications–Towards Networked Li-Fi*. Cambridge, U.K.: Cambridge Univ. Press, 2015.
[2] S. Arnon Ed., *Visible Light Communication*. Cambridge, U.K.: Cambridge Univ. Press, 2015.
[3] Z. Ghassemlooy, L. N. Alves, S. Zvanovec, and M.-A. Khalighi Eds., *Visible Light Communications: Theory and Applications*. Boca Raton, FL, USA: CRC Press, 2017.
[4] P. A. Hoeher, *Visible Light Communications–Theoretical and Practical Foundations*. Munich, Germany: Hanser Publishers, 2019.
[5] S. Arnon, J. Barry, G. Karagiannidis, R. Schober, and M. Uysal Eds., *Advanced Optical Wireless Communication Systems*. Cambridge, U.K.: Cambridge Univ. Press, 2012.
[6] M. Uysal, C. Capsoni, Z. Ghassemlooy, A. Boucouvalas, and E. Udvary Eds., *Optical Wireless Communications: An Emerging Technology*. Berlin, Germany: Springer, 2016.
[7] M. Z. Chowdhury, M. T. Hossan, A. Islam, and Y. M. Yang, "A comparative survey of optical wireless technologies: Architectures and applications," *IEEE Access*, vol. 6, pp. 9819–9840, 2018.
[8] ITU, "Recommendation ITU-T G.9991 High-speed indoor visible light communication transceiver–System architecture, physical layer and data link layer specification," Mar. 2019.
[9] *IEEE standard for local and metropolitan area networks–Part 15.7: Short-range wireless optical communication using visible light*, IEEE 802.15.7-2018, Apr. 2019.
[10] R. Zia-ul-Mustafa et al., "Quantum key distribution for visible light communications: A review," in *Proc. 13th Int. Symp. Commun. Syst., Netw. Digit. Signal Process.* 2022, pp. 589–594.
[11] L. Zeng et al., "High data rate multiple input multiple output (MIMO) optical wireless communications using white LED lighting," *IEEE J. Sel. Areas Commun.*, vol. 27, no. 9, pp. 1654–1662, Dec. 2009.
[12] K. Lee, H. Park, and J. R. Barry, "Indoor channel characteristics for visible light communications," *IEEE Commun. Lett.*, vol. 15, no. 2, pp. 217–219, Feb. 2011.
[13] S. P. Rodríguez, R. P. Jiménez, B. R. Mendoza, F. J. L. Hernández, and A. J. A. Alfonso, "Simulation of impulse response for indoor visible light communications using 3D CAD models," *EURASIP J. Wireless Commun. Netw.*, vol. 2013, pp. 1–10, Feb. 2013, doi: 10.1186/1687-1499-2013-7.
[14] A. Tsiatmas, C. P. M. J. Baggen, F. M. J. Willems, J.-P. M. G. Linnartz, and J. W. M. Bergmans, "An illumination perspective on visible light communications," *IEEE Commun. Mag.*, vol. 52, no. 7, pp. 64–71, Jul. 2014.
[15] H. Schulze, "Frequency-domain simulation of the indoor wireless optical communication channel," *IEEE Trans. Commun.*, vol. 64, no. 6, pp. 2551–2562, Jun. 2016.
[16] H. Huang, J. Wang, J. Yang, J. Xiong, and G. Gui, "Symbol error rate performance analysis of non- orthogonal multiple access for visible light communications," *China Commun.*, vol. 14, no. 12, pp. 153–161, Dec. 2017.
[17] L. Hua, Y. Zhuang, L. Qi, J. Yang, and L. Shi, "Noise analysis and modeling in visible light communication using Allan variance," *IEEE Access*, vol. 6, pp. 74320–74327, 2018.
[18] H. Schulze, "FEM simulations for the wireless optical indoor communication channel," *IET Optoelectron.*, vol. 12, no. 2, pp. 94–105, Dec. 2018.
[19] A. Kumar and S. K. Ghorai, "Performance of MIMO-VLC system for different radiation patterns of LED in indoor optical wireless communication system," in *Proc. IEEE Int. Conf. Adv. Netw. Telecommun. Syst.*, 2019, pp. 1–5.
[20] R. Raj, S. Jaiswal, and A. Dixit, "On the effect of multipath reflections in indoor visible light communication links: Channel Characterization and BER Analysis," *IEEE Access*, vol. 8, pp. 190620–190636, 2020.
[21] S. Li, A. Pandharipande, and F. M. J. Willems, "Daylight sensing LED lighting system," *IEEE Sensors J.*, vol. 16, no. 9, pp. 3216–3223, May 2016.
[22] "ReluxDesktop light planning software (Relux Informatik AG)," 2022. [Online]. Available: https://reluxnet.relux.com/en/
[23] "OpticStudio optical, illumination, and laser system design software (Zemax)," 2022. [Online]. Available: https://www.zemax.com/pages/opticstudio
[24] "DIALux lighting design software (DIAL)," 2022. [Online]. Available: https://www.dialux.com/
[25] F. Miramirkhani and M. Uysal, "Channel modeling and characterization for visible light communications," *IEEE Photon. J.*, vol. 7, no. 6, Dec. 2015, Art. no. 7905616.
[26] M. Uysal, F. Miramirkhani, O. Narmanlioglu, T. Baykas, and E. Panayirci, "IEEE 802.15.7r1 reference channel models for visible light communications," *IEEE Commun. Mag.*, vol. 52, no. 1, pp. 212–217, Jan. 2017.
[27] J. Grubor, S. Chong, J. Lee, K.-D. Langer, T. Koonen, and J. W. Walewski, "Wireless high-speed data transmission with phosphorescent white-light LEDs," in *Proc. 33rd Eur. Conf. Exhib. Opt. Commun. – Post-Deadline Papers*, 2007, pp. 1–2.
[28] G. J. M. Forkel, A. Krohn, and P. A. Hoeher, "Optical interference suppression based on LCD-filtering," *Appl. Sci.*, vol. 9, no. 15, Aug. 2019, Art. no. 3134.
[29] A. Krohn, S. Pachnicke, and P. A. Hoeher, "Genetic optimization of liquid crystal matrix based interference suppression for VLC MIMO transmissions," *IEEE Photon. J.*, vol. 14, no. 1, pp. 1–5, Feb. 2022, Art. no. 7300705.
[30] D. P. Greenberg and M. F. Cohen, "A radiosity solution for complex environments," *Comput. Graph.*, vol. 19, no. 3, pp. 31–40, Jul. 1985.
[31] C. Liedtke, CIE Test Cases. Bewertung der Genauigkeit softwarebasierter Lichtberechnung. (Ed.: Deutsche Lichttechnische Gesellschaft e.V. (LiTG), Technische Universität Berlin), Feb. 2014. [Online]. Available: http://dx.doi.org/10.14279/depositonce-8493
[32] C. A. Bouroussis, D. T. Nikolaou, and F. V. Topalis, "Test report on the validation of Relux Desktop 2019 against CIE 171:2006," May 2019. [Online]. Available: https://relux.com/assets/static/global/documents/ReluxDesktop_validation_report_Final.pdf
[33] M. Bass, J. M. Enoch, E. Van Stryland, and W. Wolfe Eds., *Handbook of Optics – Vol. III: Classical Optics, Vision Optics, X-Ray Optics*. New York, NY, USA: McGraw-Hill, 2000.
[34] J. M. Kahn and J. R. Barry, "Wireless infrared communications," *Proc. IEEE*, vol. 85, no. 2, pp. 265–298, Feb. 1997.

[35] Hamamatsu Photonics K. K., Si PIN photodiodes, S3590 series, 2020. [Online]. Available: https://www.hamamatsu.com/resources/pdf/ssd/s3590-08_etc_kpin1052e.pdf
[36] ISO/ CIE, "Spatial distribution of daylight - CIE standard general sky," Joint ISO/CIE Standard ISO 15469:2004 (E)/CIE S. 011/E:2003.
[37] S. Rajagopal, R. D. Roberts, and S.-K. Lim, "IEEE 802.15.7 visible light communication: Modulation schemes and dimming support," *IEEE Commun. Mag.*, vol. 50, no. 3, pp. 72–82, Mar. 2012.
[38] R. Lenk and C. Lenk, *Practical Lighting Design With LEDs*, 2nd ed. New York, NY, USA: Wiley, 2017.
[39] J. G. Proakis and M. Salehi, *Digital Communications*, 5th ed. New York, NY, USA: McGraw-Hill, 2008.
[40] M. Rea Ed., *Illumination Engineering Society of North America (IESNA) Lighting Handbook–Reference & Application*, 9th ed. New York, NY, USA: IESNA, 2000.
[41] "Lumileds Holding B. V., DS68 LUXEON Rebel Color Line Product Datasheet," 2017. [Online]. Available: https://www.lumileds.com/wp-content/uploads/files/DS68.pdf
[42] J. Schanda, *Colorimetry: Understanding the CIE System*. Hoboken, NJ, USA: Wiley, 2007.
[43] J. R. Barry, J. M. Kahn, W. J. Krause, E. A. Lee, and D. G. Messerschmidt, "Simulation of multipath impulse response for indoor wireless optical channels," *IEEE J. Sel. Areas Commun.*, vol. 11, no. 3, pp. 367–379, Apr. 1993.
[44] V. Jungnickel, V. Pohl, S. Noennig, and C. von Helmolt, "A physical model of the wireless infrared communication channel," *IEEE J. Sel. Areas Commun.*, vol. 20, no. 3, pp. 631–640, Apr. 2002.
[45] "Deutsche Lichttechnische Gesellschaft e.V. (LiTG), LVK Generator," Dec. 2016. [Online]. Available: https://www.litg.de/de_DE/?p=567&download=1&pid=42&
[46] N. Alshaer, M. E. Nasr, and T. Ismail, "Hybrid MPPM-BB84 quantum key distribution over FSO channel considering atmospheric turbulence and pointing errors," *IEEE Photon. J.*, vol. 13, no. 6, pp. 1–9, Dec. 2021, Art. no. 7600109.
[47] H. Schulze and P. A. Hoeher, "On the general error event probability evaluation of optical intensity modulation schemes," *IEEE Photon. J.*, vol. 14, no. 5, pp. 1–8, Oct. 2022, doi: 10.1109/JPHOT.2022.3207834.